Raman scattering from GaSb/AlSb superlattices: Acoustic, optical, and interface vibrational modes

P. V. Santos, A. K. Sood,* M. Cardona, and K. Ploog
Max-Planck-Institut für Festkörperforschung, Heisenbergstrasse 1, Postfach 80 06 65, D-7000 Stuttgart 80, Federal Republic of Germany

Y. Ohmori and H. Okamoto
Musashino Electrical Communication Laboratory, Nippon Telephone and Telegraph Corporation, 3-9-11 Midori-cho, Musashino-shi, Tokyo 180, Japan
(Received 11 August 1987)

We report a detailed Raman study of folded acoustic phonons, confined optical phonons, and interface vibrational modes in GaSb/AlSb superlattices grown on [001]-oriented GaSb substrates. A number of unusual features are observed in the intensity dependence of the Raman lines on the incident laser energy, for laser excitations ranging from the electronic transition energies E_1 of GaSb to E_0 of AlSb.

I. INTRODUCTION

The vibrational properties of semiconductor superlattices, particularly of $GaAs/Al_xGa_{1-x}As$, have been studied extensively in the recent past by Raman scattering.[1,2] It has been shown that the periodicity of the superlattice (SL) gives rise to the Brillouin-zone folding of the acoustic-phonon branch,[3,4] whereas the optical phonons can be described as folded or confined depending on the overlap of the optical-mode frequencies of the two constituent materials of the superlattice.[5,6] In addition, electrostatic interface vibrational modes exist which propagate along the layers as well as in the direction perpendicular to the layer planes.[7]

So far, much of the reported work has been done on almost-lattice-matched $GaAs/Al_xGa_{1-x}As$ systems. In this paper we report a detailed study of phonons in GaSb/AlSb systems which come under the classification of strained-layer superlattices. Recently, the Raman shifts of both GaSb and AlSb longitudinal-optical (LO) phonons in these superlattices have been utilized to determine strains needed to accommodate the 0.65% lattice mismatch.[8,9] The electronic structure has been analyzed by electroreflectance,[10] luminescence,[10,11] and optical absorption,[12] showing the formation of subbands at the Γ point (type-I superlattice, i.e., band-edge modulation has opposite sign for conduction and valence bands). Resonance Raman experiments have been done near the E_1 edge of GaSb in order to investigate the electronic structure in the region of the Brillouin zone near the L point.[13]

The samples studied here include short-period GaSb/AlSb superlattices grown by molecular-beam epitaxy on [001]-oriented GaSb substrates. As in $GaAs/Al_{1-x}Ga_xAs$ superlattices, Raman scattering from folded phonons, confined optical phonons, and interface vibrational modes is observed. However, a number of unusual features are seen in the Raman spectra for excitation energies ranging from the critical point E_1 of bulk GaSb (denoted $E_1^{GaSb}=2.16$ eV at 77 K) to the critical point E_0 of bulk AlSb ($E_0^{AlSb}=2.32$ eV). Three types of resonancelike behaviors—denoted α, β, and γ—were identified in the intensity dependence of the Raman lines on the excitation energy. They are listed below.

(i) Resonance α lies near E_1^{GaSb} and is characterized by an increase in the intensity of the higher-order, folded, longitudinal-acoustic- (LA-) phonon lines and of the GaSb-like transverse-optical (TO) line. The relative intensities of the folded acoustic-phonon doublets near this resonance do not agree with the calculations based on the elastic-continuum model (ECM).[4,14] The observed frequencies of the higher-order folded phonons also do not match the predictions[4,15] of the ECM, but rather agree better with the linear-chain model (LCM).[4]

(ii) Resonance β lies at an energy $E_1^{GaSb,SL}$ that depends on the thickness of the GaSb layers. This resonance is possibly due to the splitting of the E_1^{GaSb} transition due to quantum-size effects. For excitation near $E_1^{GaSb,SL}$, a strong and asymmetric Raman line is observed at the high-frequency cutoff of the folded LA dispersion corresponding to the highest-order folded-phonon doublet. The frequency of this line also corresponds to zone-edge (X-point) phonons in bulk GaSb and AlSb. Other strong lines that can be related to maxima in the phonon density of states appear in the Raman spectrum for excitation near resonance β. They result from scattering mechanisms without wave-vector conservation.

(iii) Finally, resonance γ is assigned to the critical point $E_0^{AlSb,SL}$ of the AlSb layers corresponding to E_0 in bulk AlSb. The Raman spectra for excitation near this resonance show an enhancement in the intensity of both the GaSb-like and AlSb-like optical-phonon lines.

The outline of this paper is as follows. Section II deals with experimental details. In Sec. III we present and discuss Raman scattering results on confined optic, interface, and acoustic phonons. Section IV contains the summary and conclusions.

II. EXPERIMENT

The samples investigated here are three GaSb/AlSb superlattices grown by molecular-beam epitaxy (MBE) on [001]-oriented GaSb substrates. The sample parameters are listed in Table I. They were estimated from the growth rates and x-ray measurements,[16] as will be discussed below.

The GaSb/AlSb superlattices belong to the so-called strained-layer superlattices due to the 0.65% difference in the lattice constants of GaSb and AlSb. In our samples, the magnitude of the strain in the superlattice layers was determined by double-crystal x-ray-diffraction measurements. Figure 1 shows the diffraction pattern of sample A measured near the (004) reflex of GaSb using the Cu $K\alpha_1$ line as an incoming x-ray beam ($\lambda=1.54056$ Å). The strongest peak is the GaSb (004) reflex located at a diffraction angle of $\theta_0+\delta\theta_0=0.5299$ rad. The main superlattice reflex at $\delta\theta=0$ is shifted towards smaller angles with respect to the substrate peak. It corresponds to an average lattice constant $\bar{a}^{\perp}$ in the direction perpendicular to the layers (z direction), given by[16]

$$\bar{a}^{\perp}=a_1[1-(\cot\theta_0)\,\delta\theta_0]\ , \tag{1a}$$

equal to 6.1261 Å for sample A. Here, a_1 is the lattice constant of bulk GaSb. $\bar{a}^{\perp}$ is further modulated along z, following the periodic alternation of layers. This is evidenced by the small satellite peaks at $\delta\theta_{\pm1}=\pm32.4$ mrad away from the main superlattice reflex in Fig. 1 (only the $\delta\theta_{+1}$ satellite is shown in Fig. 1). The position of these satellites yields the superlattice period

$$d=\bar{a}^{\perp}[1-(\cot\theta_0)\,\delta\theta_{+1}] \tag{1b}$$

listed in Table I.

The intensity of the satellite $\delta\theta_{\pm1}$ is related to the modulation amplitude of $a^{\perp}(z)$. Assuming $\bar{a}^{\perp}(z)$ to have a square modulation profile, the average stress in the superlattice layers can be determined from the x-ray data. In this case, the GaSb- (AlSb-) layer lattice constants $a_1^{\perp}$ ($a_2^{\perp}$) along z are related to the average lattice constant $\bar{a}^{\perp}$ by[8]

$$\bar{a}^{\perp}=\frac{d_1a_1^{\perp}+d_2a_2^{\perp}}{d_1+d_2}$$

$$=\frac{d_1}{d_1+d_2}a_1(1+\varepsilon_1^{\perp})+\frac{d_2}{d_1+d_2}a_2(1+\varepsilon_2^{\perp})\ , \tag{2}$$

where the a_i, $i=1,2$, are the bulk lattice constants, and $\varepsilon_i^{\perp}=(a_i^{\perp}-a_i)/a_i$ are the strains along z. Here and in the following the indices 1 and 2 denote the GaSb and AlSb layers, respectively.

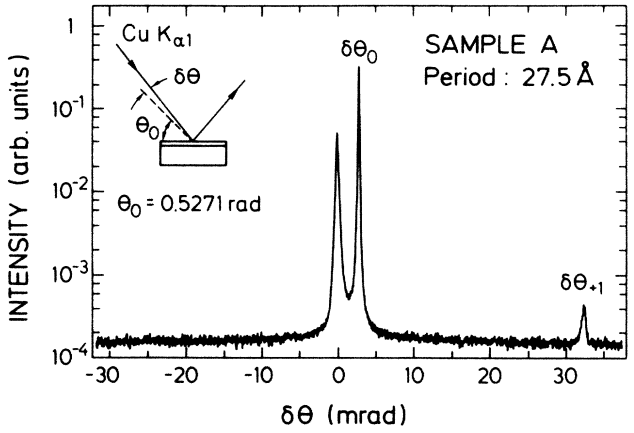

FIG. 1. X-ray-diffraction pattern of sample A measured with the Cu $K\alpha_1$ line ($\lambda=1.54056$ Å). The zero point of the relative angle scale corresponds to $\theta_0=0.5271$ rad. The peak at $\delta\theta=0$ is the main superlattice (004) reflex and that at $\delta\theta_0$ is the corresponding reflex from the GaSb substrate. The small peak at $\delta\theta_{+1}$ is related to the artificial periodicity of the superlattice.

In the layer plane the corresponding lattice constants are equal as a consequence of the coherent growth:

$$a_1^{\parallel}-a_2^{\parallel}=a_1(1+\varepsilon_1^{\parallel})-a_2(1+\varepsilon_2^{\parallel})=0\ . \tag{3}$$

The strains $\varepsilon_i^{\parallel}$ and $\varepsilon_i^{\perp}$ are related to the "biaxial" stress X_i by the elastic compliances $s_{11,i}$ and $s_{12,i}$:

$$\varepsilon_i^{\perp}=2s_{12,i}X_i\ , \tag{4}$$

$$\varepsilon_i^{\parallel}=(s_{11,i}+s_{12,i})X_i\ . \tag{5}$$

Equations (1)–(5), solved simultaneously, yield the biaxial stress X_i in the in-layer plane of the GaSb and AlSb layers. In columns 6 and 7 of Table I are compiled the results for samples A, B, and C, which were calculated using the material constants listed in Table II. As the samples have been grown on a GaSb substrate and the thickness of each AlSb layer is less than the critical thickness t_c above which misfit dislocations appear ($t_c\approx3000$ Å is a rough estimate from Fig. 1 of Ref. 17), the GaSb layers are expected to be unstrained and the AlSb layers to be under compression. In fact, for sample C, where the GaSb layers are much thicker than the AlSb ones ($d_1\approx4d_2$), the stress in the GaSb is practically zero. The results for samples A and B, where nominally $d_1=d_2$, show, however, that although the stress is larger in the AlSb layers, the GaSb layers are also strained. We con-

TABLE I. Samples investigated in this work. The indices 1 and 2 correspond to the GaSb and AlSb layers, respectively.

Sample	d (Å)	d_1 (Å)	d_2 (Å)	No. of periods	X_1 (10^9 dyn/cm^2)	X_2 (10^9 dyn/cm^2)	$\Delta\omega_1^{LO}$ (cm^{-1})	$\Delta\omega_2^{LO}$ (cm^{-1})
A	27.5	13.7	13.7	200	1.6±0.6	−4.2±0.6	−0.6±0.2	3.0±0.5
B	53.4	26.7	26.7	100	1.7±0.6	−4.2±0.7	−0.6±0.3	3.0±0.5
C	160	130	30	50	0.08	−5.0	−0.03	4.0

TABLE II. Lattice properties of GaSb and AlSb at 300 K (Ref. 18).

	Lattice constant (Å)	ρ (g/cm^3)	v (10^5 cm/s)	$s_{11,i}$ (10^{-12} cm^2/dyn)	$s_{12,i}$ (10^{-12} cm^2/dyn)
GaSb	6.0959	5.614	3.97	1.582	−0.496
AlSb	6.1355	4.26	4.53	1.696	−0.562

clude, therefore, that the stress is partially relaxed as one moves away from the superlattice-substrate interface. Furthermore, as we have always observed sharp superlattice (004) reflexes (see peak at $\delta\theta_0$ in Fig. 1), the region where the stress relaxes must be much thinner than the total superlattice thickness. Due to the large absorption coefficient of the superlattices to visible light, this region has not been accessed in our Raman measurements.

Raman measurements were performed at various temperatures between 5 and 300 K in backscattering geometry using various lines of an Ar^+ and a Kr^+ laser, with typical powers ranging from 100 to 300 mW. The power density on the sample was reduced using a slit focus (cylindrical condenser). The scattering geometries employed were $z(xx)\bar{z}$ (denoted by XX hereafter) and $z(yx)\bar{z}$ (denoted by YX) with x, y, and z parallel to the [100], [010], and [001] directions of the cubic crystal, respectively.

III. RESULTS AND DISCUSSION

A. Excitation energy dependence of the Raman spectra

Raman experiments on the GaSb/AlSb superlattices were performed with incident laser photon energies $\hbar\omega_L$ ranging from 1.65 to 2.57 eV. The relevant direct electronic transitions in this energy range are centered around the Γ point and along the Λ line of the Brillouin zone in GaSb and AlSb:[18] $E_0^{\mathrm{GaSb}}(\Gamma_{8v}-\Gamma_{6c})=0.78$ eV (0.70 eV) at 77 K (300 K), $E_0^{\mathrm{AlSb}}(\Gamma_{15v}-\Gamma_{1c})=2.32$ eV (2.22 eV), $E_1^{\mathrm{GaSb}}(\Lambda_{4,5v}-\Lambda_{6c})=2.16$ eV (2.03 eV), $(E_1+\Delta_1)^{\mathrm{GaSb}}(\Lambda_{4,5v}-\Lambda_{6c})=2.60$ eV (2.47 eV), and $E_1^{\mathrm{AlSb}}(\Lambda_{4,5v}-\Lambda_{6c})=2.86$ eV (2.78 eV).

In a superlattice structure one expects a shift in the position of the critical points of the bulk materials due to quantum-size effects. In addition, calculations for small-period superlattices (see, for instance, Ref. 19) show that the electronic branches of the individual materials mix in an intricate way to form the superlattice energy bands. In this case the band structure of the superlattice no longer resembles that of the bulk material.

Since the electronic structure of GaSb/AlSb superlattices at the L point (or along the Λ line) is not well understood,[13] we are not in a position to identify *a priori* the resonances with the electronic transitions. In order to get information about the electronic structure of the samples near the L point, the energy dependence of the complex pseudodielectric constant was measured by ellipsometry at room temperature. Figure 2 shows the imaginary part (ϵ_I) of the pseudodielectic constant of samples B [Fig. 2(b)] and A [Fig. 2(c)] for photon energies ranging from 1.5 to 2.8 eV. Figure 2(a) is the corresponding curve for bulk GaSb. The oscillations below 2 eV in Figs. 2(b) and 2(c) are due to interference fringes associated with the total thickness of the superlattice. They disappear at 1.9±0.1 eV for sample A and at 1.8±0.1 eV for sample B as a result of the increase in light absorption. The two peaks in the ϵ_I spectrum of bulk GaSb [Fig. 2(a)] are related to the critical points $E_1^{\mathrm{GaSb}}=2.03$ eV and $(E_1+\Delta_1)^{\mathrm{GaSb}}=2.47$ eV. Similar structures are observed in Figs. 2(b) and 2(c): we assign them to two new critical points, $E_1^{\mathrm{GaSb,SL}}$ and $(E_1+\Delta_1)^{\mathrm{GaSb,SL}}$, respectively, of the GaSb layers in the superlattice. The exact critical energies were determined, for each sample, by a fitting procedure, and are indicated by arrows in Fig. 2.

The critical points $E_1^{\mathrm{GaSb,SL}}$ and $(E_1+\Delta_1)^{\mathrm{GaSb,SL}}$ are

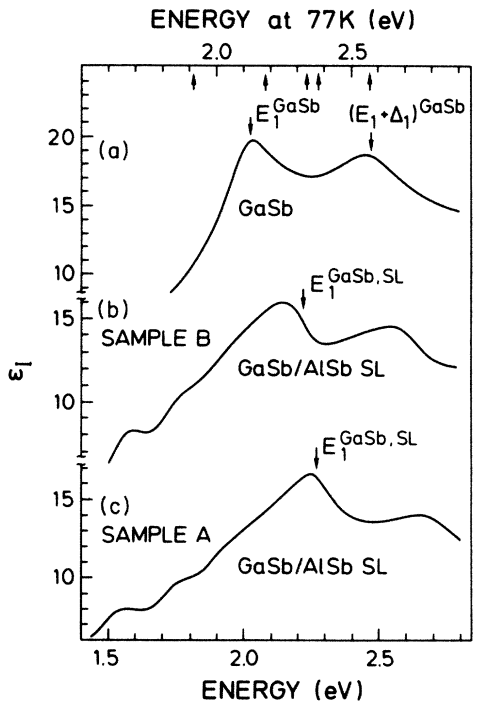

FIG. 2. Energy dependence of the imaginary part ϵ_I of the pseudodielectric constant for (a) a GaSb substrate, (b) sample B, and (c) sample A measured by ellipsometry at room temperature. The arrows on the curves indicate the position of the critical points E_1^{GaSb} and $E_1^{\mathrm{GaSb,SL}}$. The upper scale of the plot gives the calculated position to the corresponding critical points at 77 K (for details, see text). The arrows on this scale indicate the excitation energies used to record the Raman spectra of Figs. 3 and 4. The samples were not chemically etched so as to avoid damage of the superlattice. No correction for oxide surface layer was performed. Hence the data for GaSb differ somewhat from those of Ref. 31.

shifted towards higher energies with respect to the E_1^{GaSb} of bulk GaSb. The position in energy of $E_1^{GaSb,SL}$ depends on the GaSb-layer thickness: in sample B ($d_1 = 26.7$ Å), $E_1^{GaSb,SL} = 2.22$ eV, whereas in sample A ($d_1 = 13.7$ Å), $E_1^{GaSb,SL} = 2.27$ eV. Both structures in the ϵ_I spectra of the superlattices are broader than in the bulk material. In addition, the peak corresponding to $E_1^{GaSb,SL}$ is asymmetric with a low-energy tail which overlaps E_1^{GaSb}. This tail may be associated with a second peak lying close to E_1^{GaSb}. Such a splitting of the E_1 critical point has recently been observed for the GaAs-like E_1 transition in small-period GaAs/AlAs superlattices.[20]

Figure 3 shows Raman spectra of sample A recorded with different excitation energies in the *XX* (left-hand side) and *YX* (right-hand side) scattering configurations. Figure 4 displays the corresponding spectra for sample B. In these measurements the samples were kept at liquid-nitrogen temperature, except for the heating due to light absorption. The photon energies of the exciting lines, indicated by arrows in the upper scale of Fig. 2, lie around the critical point $E_1^{GaSb,SL}$. This scale was constructed assuming a temperature variation of the superlattice critical points $E_1^{GaSb,SL}$ and $(E_1+\Delta_1)^{GaSb,SL}$ equal to that of the corresponding critical point in bulk GaSb (~ -0.46 meV/K between 77 and 300 K, from Ref. 18). In order to allow a direct comparison of the Raman intensities, the count rate of each spectrum was normalized with respect to the scattering intensity of a CaF_2 crystal used as a reference.[21]

For the purpose of analysis, each spectrum can be divided into three main spectral regions.

(i) *Acoustic region:* For Raman shifts $\omega < 200$ cm^{-1} there is a series of lines corresponding to the excitation of folded longitudinal-acoustic (LA) phonons propagating perpendicular to the superlattice layers. The lines are stronger in the *XX* configuration and appear as doublets labeled $m = \pm 1, \pm 2, \ldots, \pm 8$ that are unresolved in Figs.

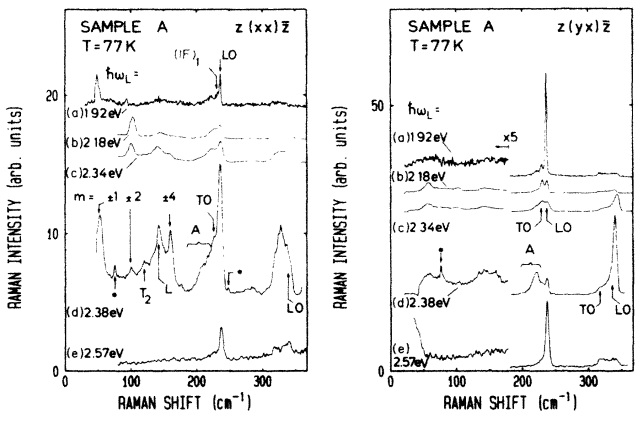

FIG. 3. Raman spectra for sample A measured at 77 K for different excitation energies in the *XX* (left-hand side) and *YX* (right-hand side) configurations. The Raman intensity in each spectrum was normalized with respect to the scattering intensity of the optical phonon in CaF_2. The asterisks indicate laser plasma lines.

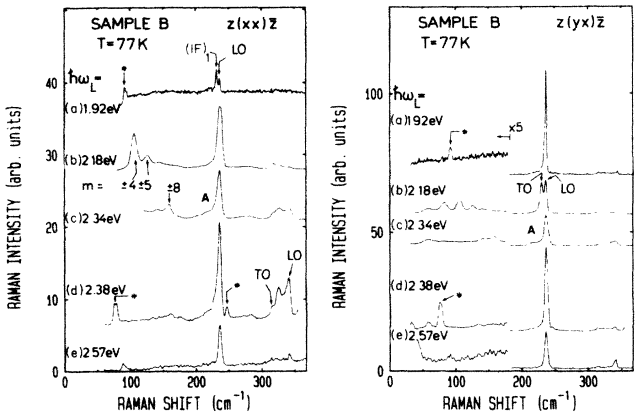

FIG. 4. Raman spectra for sample B measured at 77 K for different excitation energies in the *XX* (left-hand side) and *YX* (right-hand side) configurations. The Raman intensity in each spectrum was normalized with respect to the scattering intensity of the optical phonon in CaF_2. The asterisks indicate laser plasma lines.

3 and 4. The lines marked T_2 and L are assigned to maxima in the acoustic-phonon density of states, as will be discussed in Sec. III C.

(ii) *GaSb optical region:* For $200 < \omega < 250$ cm^{-1} the spectra show lines related to the excitation of longitudinal-optical (LO) and transverse-optical (TO) phonons confined in the GaSb layers. The Raman spectra also show additional lines related to the excitation of interface modes [$(IF)_1$ in Figs. 3 and 4] that propagate along the superlattice interfaces.[7] The structures denoted by *A* correspond to maxima in the density of states for optical phonons in GaSb, occurring roughly at the boundary of the crystal Brillouin zone.[22]

(iii) *AlSb optical region:* In the spectral region $300 < \omega < 350$ cm^{-1} the Raman spectra exhibit lines associated with optical modes confined to the AlSb layers and AlSb-like interface modes.[7]

The intensity of the Raman signal from the GaSb (200–250 cm^{-1}) and the AlSb layers (300–350 cm^{-1}) in Figs. 3 and 4 reaches a maximum for $\hbar\omega_\gamma = 2.38$ eV. This result also holds for sample C, which has a much larger period ($d = 160$ Å). [Note, however, the exception of the LO line of GaSb is sample A in the $z(yx)\bar{z}$ configuration, which has increased at 2.57 eV. We have not studied this anomaly in detail, but it may result from an interference of the E_0^{AlSb} and $(E_1+\Delta_1)^{GaSb}$ resonances. We believe, however, that the $z(xx)\bar{z}$ configuration gives a better measurement of the resonance energies since it is sharper.[23]] In the following, we shall refer to this behavior at $\hbar\omega_\gamma = 2.38$ eV as resonance γ. Resonance γ in sample B lies above the critical point $E_1^{GaSb,SL}$, as indicated in the upper scale of Fig. 2. For sample A it practically coincides with $E_1^{GaSb,SL}$. However, the fact that resonance γ occurs at the same energy in all samples independent of the GaSb-layer thickness suggests that it is probably not related to the GaSb layers but to the critical point $E_0^{AlSb,SL}$ of the AlSb layers corresponding to $E_0^{AlSb} = 2.32$ eV (at 77 K) in bulk AlSb. The electronic

states involved in this resonance must also extend over the GaSb superlattice layers as both GaSb-like and AlSb-like phonons resonate at $\hbar\omega_\gamma$.

As the Raman measurements were restricted to a small set of discrete laser lines, it is not possible to establish precisely the position of resonance γ. From the spectra of Figs. 3 and 4, however, we estimate that $\hbar\omega_\gamma$ certainly lies above 2.36 eV, i.e., at least 40 meV above E_0^{AlSb}. This shift may be partially accounted for by an outgoing resonance.[23] A second contribution to the shift should arise from the biaxial stress in the AlSb layers. This stress can be decomposed into a hydrostatic plus a pure shear component along z. The hydrostatic component leads to an increase in the band gap of AlSb, while the shear component causes a splitting of that gap. The shift in the light-hole–to–conduction-band transition energy, $\Delta E_{0,\mathrm{LH}}^{\mathrm{AlSb}}$ is[24]

$$\Delta E_{0,\mathrm{LH}}^{\mathrm{AlSb}} = [2a(s_{11,2}+2s_{12,2})+b(s_{11,2}-s_{12,2})]X_2 = 50 \text{ meV} , \quad (6)$$

and

$$\Delta E_{0,\mathrm{HH}}^{\mathrm{AlSb}} = [2a(s_{11,2}+2s_{12,2})-b(s_{11,2}-s_{12,2})]X_2 = 15 \text{ meV} \quad (7)$$

for the heavy-hole–to–conduction-band transition $\Delta E_{0,\mathrm{HH}}^{\mathrm{AlSb}}$ in sample A. $\Delta E_{0,\mathrm{HH}}^{\mathrm{AlSb}}$ values of 15 and 20 meV were obtained for samples B and C, respectively. In the previous expressions, a and b are the deformation potentials for the E_0 critical point of AlSb.[18] The critical point $E_0^{\mathrm{AlSb,SL}}$ should therefore be at least 15 meV above E_0^{AlSb}, on account of the biaxial strain.

For laser photon energies near E_1^{GaSb} ($\hbar\omega_L = 2.18$ eV in Figs. 3 and 4) the intensity of the higher-order acoustic-phonon doublets ($m = \pm 2$ in Fig. 3 and $m = \pm 4$ and ± 5 in Fig. 4) is strongly enhanced in comparison with the other lines. These folded doublets are also present in the YX spectrum, which shows an intense line attributed to the TO-like phonons from the GaSb layers. We shall denote this behavior at $\hbar\omega_\alpha \approx E_1^{\mathrm{GaSb}}$ as resonance α. Note that $\hbar\omega_\alpha$ lies on the low-energy tail of the $E_1^{\mathrm{GaSb,SL}}$ structures in the ϵ_I spectra of Fig. 2.

As the laser energy is swept through the two resonances discussed above and across $E_1^{\mathrm{GaSb,SL}}$, the relative intensities of the Raman lines change. This behavior can be better followed in the high-resolution spectra for sample A shown in Fig. 5.

(i) Below the resonance α [see, for instance, curve (a)] for $\hbar\omega_L = 1.92$ eV in Fig. 5, the XX spectrum in the acoustic region only shows the first doublet $m = \pm 1$, while the YX spectrum is dominated by the LO line of the GaSb layers and has only very weak features in the acoustic region.

(ii) When the laser photon energy is increased to $\hbar\omega_\alpha$ ($\hbar\omega_L = 2.18$ eV), the acoustic doublet $m = \pm 2$ is strongly enhanced in the XX spectrum in comparison with the $m = \pm 1$ doublet. The same occurs to the intensity of the GaSb-like TO line in comparison with the LO line, in the YX spectrum. The latter spectrum also presents weak features corresponding to the first two acoustic-phonon doublets $m = \pm 1$ and ± 2.

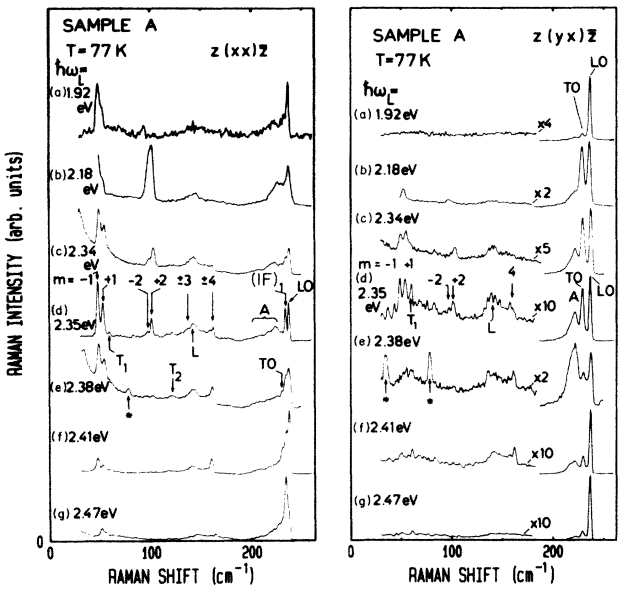

FIG. 5. High-resolution Raman spectra of sample A recorded at 77 K in the XX (left-hand side) and YX (right-hand side) scattering configurations for various excitation energies.

(iii) At $\hbar\omega_L = 2.34$ eV a weak doublet $m = \pm 3$, together with the broad line L at 140 cm^{-1}, is observed. In addition, a new line corresponding to the excitation of the $m = \pm 4$ folded-phonon doublet appears in the XX configuration. The $m = \pm 1$, ± 2, and ± 3 doublets are also excited in the YX spectrum, together with the structure denoted A in the optical-phonon region of the GaSb layers. A new line, $(\mathrm{IF})_1$, presumably a GaSb-like interface electrostatic mode, appears near the LO line in the XX spectrum.

(iv) As $\hbar\omega_L$ is raised to $\hbar\omega_\gamma$ ($\hbar\omega_L = 2.38$ eV), the intensity of the L and $m = \pm 4$ lines in the XX spectrum and of line A in the YX spectrum increase with respect to the other lines. A closer analysis of the Raman and ϵ_I spectra for sample B (Figs. 2 and 4) suggests that these lines resonate not at $\hbar\omega_\gamma$, but at an energy $\hbar\omega_\beta \approx E_1^{\mathrm{GaSb,SL}}$ $\hbar\omega_\beta$ and $\hbar\omega_\gamma$ practically coincide in sample A. The acoustic lines L and $m = \pm 4$ are also strong in the YX configuration. The acoustic doublet $m = \pm 2$ practically disappears near $\hbar\omega_\gamma$, while the intensity of the GaSb-like TO line is strongly reduced in comparison with the LO line.

(v) Above $\hbar\omega_\gamma = 2.41$ eV [curve (g) in Fig. 5] the intensity of all acoustic lines decreases, and the spectrum, in the acoustic region, becomes similar to that for $\hbar\omega_L = 1.92$ eV. The XX spectrum of the GaSb region is dominated by the interface mode $(\mathrm{IF})_1$.

The changes in the intensity of the Raman lines have thus been associated with electronic resonancelike transitions placed at $\hbar\omega_\alpha \approx E_1^{\mathrm{GaSb}}$, $\hbar\omega_\beta \approx E_1^{\mathrm{GaSb,SL}}$, and $\hbar\omega_\gamma \approx E_0^{\mathrm{AlSb,SL}}$ that are not resolved in the ϵ_I spectra of Fig. 2. The electronic states involved in each of these transitions couple in a different way to the various branches of the folded acoustic and confined optical dispersions. This point will be discussed further in the

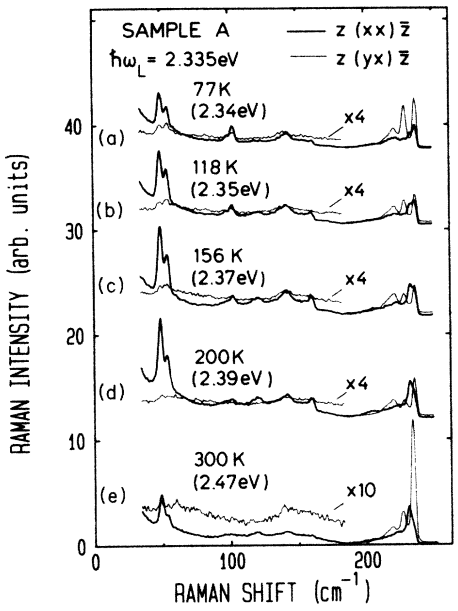

FIG. 6. Raman spectra measured at different temperatures for $\hbar\omega_L = 2.335$ eV in the XX (left-hand side) and YX (right-hand side) scattering configurations. For details, see text.

following sections. This behavior can be followed either by changing the laser energy, as in the spectra of Figs. 3–5, or, alternatively, by fixing the excitation energy and varying the sample temperature. In the latter case, coupling to the different electronic states is achieved by temperature-tuning the electronic transition to the excitation energy. This is shown in Fig. 6, where Raman spectra of sample A were recorded for $\hbar\omega_L = 2.335$ eV at different temperatures between 77 and 300 K. Assuming a temperature shift of the electronic transitions of -0.46 meV/K (Ref. 18), an effective excitation energy can be determined for every spectrum measured above 77 K. These values are shown in parentheses in Fig. 6. Note that with this effective excitation-energy scale the series of spectra of Fig. 6 also follows the behavior shown in Fig. 5.

B. Confined phonons

Since the LO-phonon branches in the bulk GaSb and AlSb do not overlap in frequency,[25,26] optical phonons will be confined in the individual layers.[6] Owing to the confinement, the phonon frequency shifts down from the value in bulk material. However, in strained-layer superlattices phonons can also shift due to the biaxial stress in the layers. Let us estimate the shift in the phonon frequency due to the stress values determined in Sec. II (see Table I). Following Refs. 8 and 27,

$$\Delta\omega_i^{\mathrm{LO}} = 2\Delta\Omega_i^H - \tfrac{2}{3}\Delta\Omega_i \ , \tag{8}$$

where

$$\Delta\Omega_i^H = \frac{X_i}{6\omega_i^{\mathrm{LO}}}(p_i + 2q_i)(s_{11,i} + 2s_{12,i} + 2s_{12,i})$$

and

$$\Delta\Omega_i = \frac{X_i}{2\omega_i^{\mathrm{LO}}}(p_i - q_i)(s_{11,i} - s_{12,i}) \ .$$

Here, ω_i^{LO} is the (unshifted) LO frequency. The experimental values $(p_i - q_i)/(\omega_i^{\mathrm{LO}})^2 = 0.44$ (0.97) and $(p_i + 2q_i)/6(\omega_i^{\mathrm{LO}})^2 = -1.1$ (-1.18) for GaSb (AlSb) were extracted from Ref. 27 (Ref. 28). The calculated LO frequency shifts are listed in Table I. Note that $\Delta\omega_i^{\mathrm{LO}}$ is small for the GaSb layers ($i = 1$), and the frequency shifts of the GaSb-like LO phonons arise mainly from their confinement. For the AlSb-like LO phonons one expects a strain-induced wave-number shift from 3.0 to 4.0 cm^{-1} towards higher wave numbers.

1. *Phonons between 200 and 250 cm^{-1} (GaSb region)*

Figure 7 shows high-resolution Raman spectra of sample A at 5 K with $\hbar\omega_L = 1.92$ and 2.41 eV. The spectrum for 1.92 eV in the YX geometry is about 7 times stronger than in the XX geometry (not shown in the figure) and corresponds to off resonance. On the other hand, for

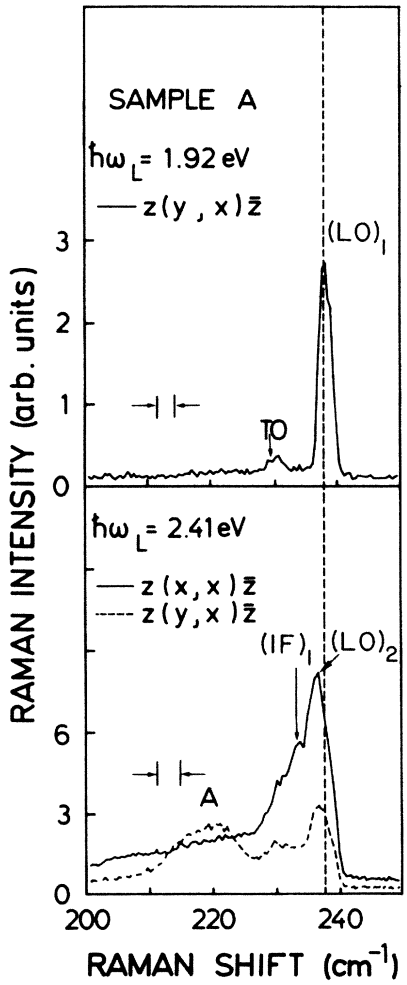

FIG. 7. Raman spectra of sample A at 5 K for $\hbar\omega_L = 1.92$ eV (off resonance) and $\hbar\omega_L = 2.41$ eV (resonance).

$\hbar\omega_L = 2.41$ eV (the laser photon energy is near the resonance γ) the ratio of the intensities in the XX and YX geometries equals about 2.5. Odd-order ($m = 1,3,5,\ldots$) optical phonons are known to be stronger in the $z(yx)\bar{z}$ geometry, whereas even-order ($m = 2,4,\ldots$) phonons dominate near resonance in the $z(xx)\bar{z}$ geometry.[6] Accordingly, the main peak $(LO)_1$ in the spectra with $\hbar\omega_L = 1.92$ eV (237.7 cm^{-1}) in Fig. 7 is assigned to $m = 1$ and that with $\hbar\omega_L = 2.41$ eV (236.6 cm^{-1}) is assigned to $m = 2$. Figure 8 shows Raman spectra for samples B, C, and bulk GaSb (arbitrary face) at 5 K with $\hbar\omega_L = 2.41$ eV. Note that for sample C ($d_1 = 130$ Å) the LO Raman shift matches that of bulk GaSb, thereby confirming that the GaSb layers in sample C are not strained.

In order to see the correspondence between the confined-phonon frequency in the GaSb layers and the bulk GaSb, we plot in Fig. 9 the observed phonon frequencies for samples A and B versus $q = 2m\pi/[(n_1 + 1)a_1]$.[29] Here, n_1 is the number of GaSb monolayers in the superlattice and $d_1 = n_1 a_1/2$ ($4 < n_1 < 5$ for sample A and $8 < n_1 < 10$ for sample B). This type of plot is justified by the fact that the nodes of the confined modes occur at the Al atoms, not at Sb.[29] A theoretical dispersion[22,25] for LO phonons along the [001] direction in bulk GaSb is also given: It was shifted up by 2.5 cm^{-1} to match the LO Raman shift in bulk GaSb at 5 K. We also show in Fig. 9 room-temperature neutron-scattering data[22] which are affected by large error bars (±6 cm^{-1}). We see from Fig. 9 that the superlattice phonons tend to be higher than the corresponding bulk phonons. Similar results have been observed for GaAs/AlAs superlattices.[6]

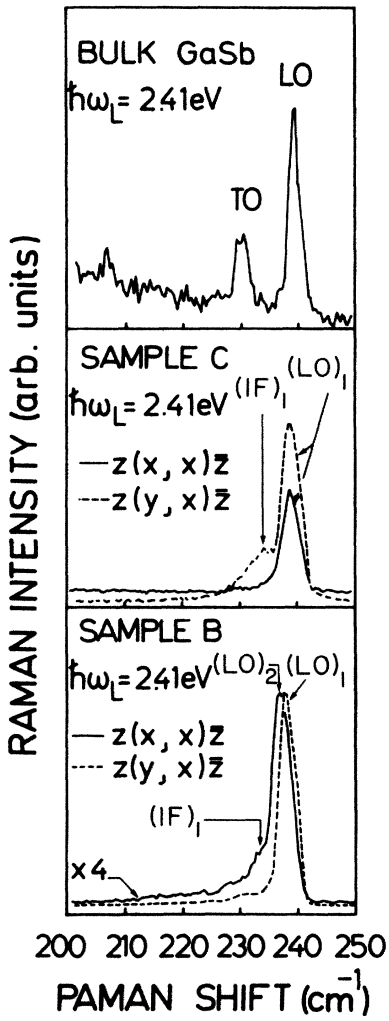

FIG. 8. Raman spectra of sample B, sample C, and bulk GaSb at 5 K for $\hbar\omega_L = 2.41$ eV.

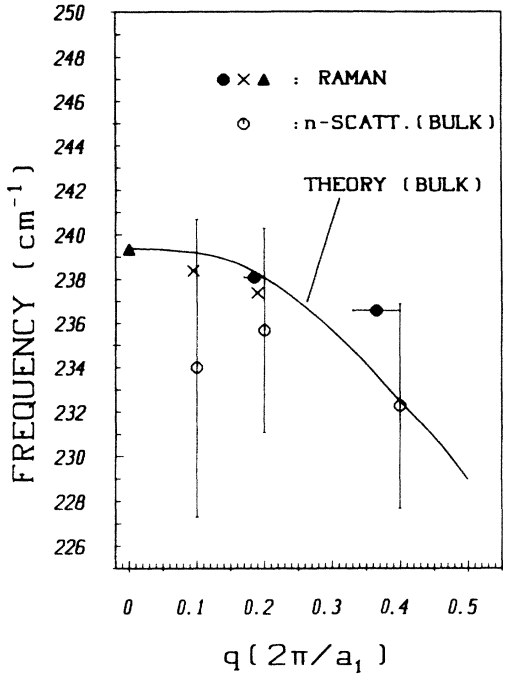

FIG. 9. Observed Raman shifts of confined phonon (solid circles for sample A and crosses for sample B) vs $2m\pi/(n_1+1)a_1$ at 5 K. The solid line is the calculated phonon dispersion in bulk GaSb (Refs. 22 and 25) at room temperature and is shifted up by 2.5 cm^{-1} to match the LO Raman shift in bulk GaSb at 5 K (solid triangle). Open circles are neutron-scattering data (Ref. 22).

The transverse-optical (TO) phonon, though forbidden in the backscattering configuration on a (001) face, appears weakly in Figs. 7 and 8. This is similar to the GaAs/AlAs case.[6] However, near resonance α ($\hbar\omega_L = 2.18$ eV in Figs. 3–5) this line becomes very strong in the YX configuration and is comparable in intensity to the LO line. The mechanism for this selection-rule violation is not clear. The origin of a broad peak between 215 and 220 cm^{-1}, labeled A in Figs. 3–5, perhaps lies in the total density of phonon states in GaSb (Refs. 22 and 25) activated by defects. In fact, this density of states for GaSb has a strong peak at $\simeq 220$ cm^{-1}.[22,25] This high density of states is produced mainly by TO phonons along [110] and [111] directions. This type of structure has been previously seen in the literature for bulk materials, specially in ternary alloys.[30] They are labeled DATO (disordered activated transverse-optical phonons).

2. *Phonons above 300 cm^{-1} (AlSb region)*

As remarked before, the AlSb layers are strained in our samples and hence LO phonons in AlSb should show a strain-induced upwards shift of 3.0±0.5 cm^{-1}, as indicated in Table I. The AlSb-like LO peak in sample A, however, has a Raman shift of 343.1 cm^{-1} (see Fig. 10) and lies, therefore, 1.3 cm^{-1} below the LO-phonon Raman shift in bulk AlSb ($\omega_2^{LO}=344.4$ cm^{-1}, Ref. 18). We attribute this downwards shift to the phonon confinement in the AlSb layers, which reduces the frequency of the LO mode. As discussed previously, this phonon corresponds to the bulk LO phonon with $q=2\pi/(n_2+1)a_2$. From the calculated AlSb phonon dispersion,[26] this mode should lie $\approx$4.1 cm^{-1} below the bulk $q=0$ LO phonon. Subtracting from this difference the stress-induced shift, we get a resulting downwards shift of 1.0±0.5 cm^{-1}. This value compares well with the shift of 1.3 cm^{-1} towards lower wave numbers determined experimentally.

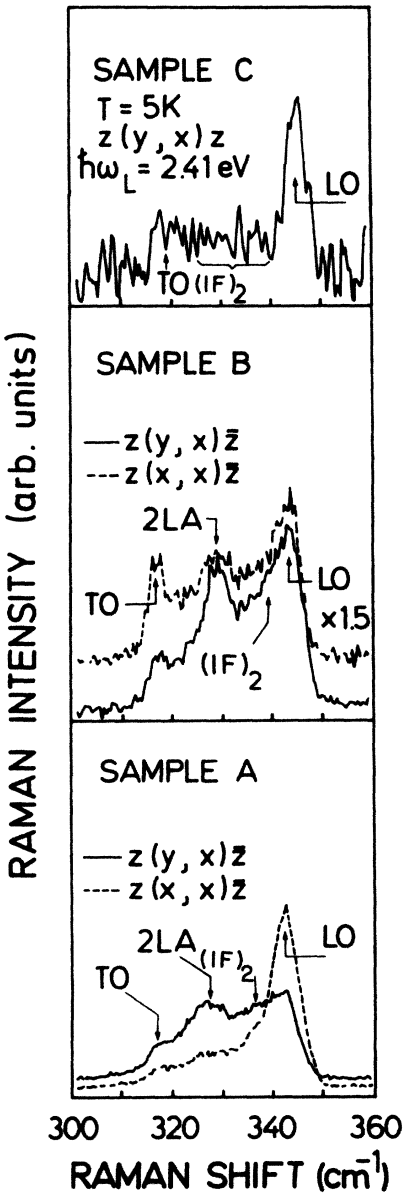

FIG. 10. Raman spectra at 5 K of the AlSb region (300–350 cm^{-1}) for samples A, B, and C.

C. Interface modes

These modes were unambiguously observed by Raman scattering in GaAs/AlAs superlattices.[7] We show similar results for GaSb/AlSb superlattices. Figure 11 depicts the calculated dispersion of the interface vibrational mode obtained with Eq. (1) of Ref. 7. The parameters used are

$$\text{GaSb: } \epsilon_1^{\infty}=14.4,\ \omega_1^{LO}=239.3\ \text{cm}^{-1},\ \omega_1^{TO}=230\ \text{cm}^{-1},$$

$$\text{AlSb: } \epsilon_2^{\infty}=10.0,\ \omega_1^{LO}=344.4\ \text{cm}^{-1},\ \omega_2^{TO}=323.4\ \text{cm}^{-1}.$$

The GaSb-like interface modes are identified as $(IF)_1$ in Figs. 7 and 8. The AlSb-like interface modes are labeled $(IF)_2$ in Fig. 10. The observed peak positions of $(IF)_1$ and $(IF)_2$ in samples A and C are indicated in Fig. 11. The + and − signs denote the symmetric and antisymmetric natures of the electrostatic potential produced by the mode with respect to the center of a GaSb layer. The symmetric mode will be seen in the *XX* configuration arising via Fröhlich interaction.[7] This is borne out by $(IF)_1$ at

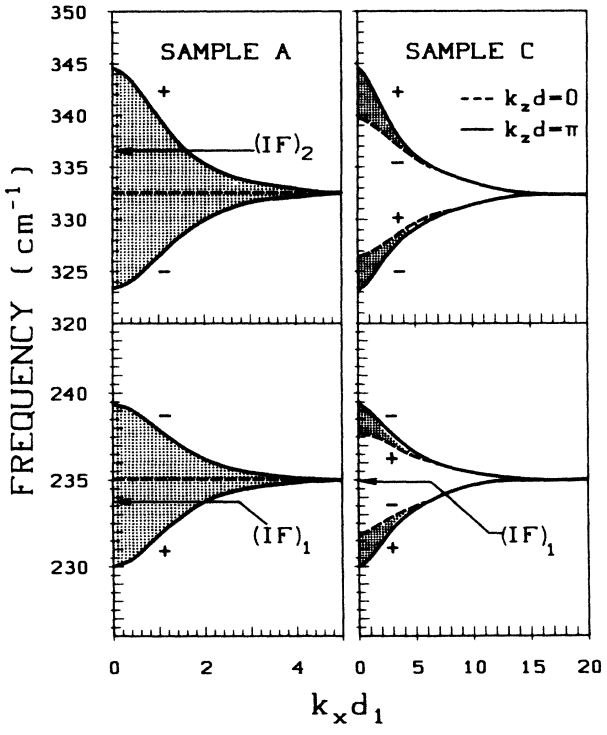

FIG. 11. Calculated dispersion of interface vibrational modes based on electrostatic model (Ref. 7). The observed modes $(IF)_1$ and $(IF)_2$ are indicated by arrows.

233.6 cm^{-1} in the $z(xx)\bar{z}$ configuration in Fig. 7 ($\hbar\omega_L = 2.41$ eV). This mode is indeed weighed towards the symmetric branch in Fig. 11. The mode $(IF)_1$ in sample C at 234.9 cm^{-1} shown in Fig. 8 appears in the $z(yx)\bar{z}$ configuration under nonresonant excitation and hence possibly involves coupling via deformation-potential interaction. The observed value corresponds to large $k_x d_1$, where there is equal admixture of symmetric and antisymmetric components [note that d_1(sample C) = 130 Å, which is $\simeq 11 d_1$(sample A), and hence large values of $k_x d_1$ are not unexpected in sample C]. Excitation of all interface modes in backscattering requires some k_x transfer, which is probably provided by interface defects or roughness.

For AlSb, interface modes are also observed (Fig. 10). However, the situation becomes complicated due to superposition of these spectra with second-order, 2LA spectra of the superlattice.

D. Folded acoustic phonons

It is well known[4] now that acoustic phonons in superlattices can propagate along the superlattice axis (z direction). The new periodicity folds the acoustic dispersion curves of an average compound at the new "mini"-Brillouin-zone edge ($q = \pm\pi/d$) and opens up small gaps at the "mini-zone" center and edges.[4]

1. Dispersion of folded acoustic phonons

The Raman lines in the acoustic frequency region correspond to longitudinal-acoustic phonons propagating along [001] with a wave vector of magnitude $q = (4\pi/\lambda_L) n_{SL}$, where n_{SL} is the average refractive index of the superlattice at the wavelength λ_L. The average dielectric constant ϵ_{SL} and therefore n_{SL} were calculated using

$$\epsilon_{SL} = (d_1\epsilon_1 + d_2\epsilon_2)/(d_1 + d_2) \ . \tag{9}$$

The values of ϵ for GaSb were taken from Ref. 31. As there is no determination of the dielectric constant of AlSb at 2.34 eV, we used the measured value at lower energy (0.8 eV) from Ref. 18. Although this leads to an underestimation of n_{SL}, we preferred this procedure to using the ellipsometrically determined values of the pseudodielectric constant since the sample surfaces were not sufficiently carefully prepared for ellipsometric work.[31] The frequencies of the folded phonons measured at 300 K for $\hbar\omega_L = 2.34$ eV in sample A ($qd = 0.27$) are shown by the crosses (×) in Fig. 12. Note that uncertainties in the determination of n_{SL} only lead to a horizontal shift in the position of the experimental points in Fig. 12 and will not affect the conclusions to be drawn in the following.

The dispersion curve for folded acoustic phonons was calculated assuming an elastic continuum model (ECM).[3] In this model each GaSb (AlSb) layer is characterized by a longitudinal sound velocity along the [001] direction v_1 (v_2) and a density ρ_1 (ρ_2). The acoustic-phonon dispersion is given by Eq. (1) of Ref. 3. The result for sample A obtained using the parameters listed in Table II (from Ref. 18) is given by the dashed line in Fig. 12. Although the

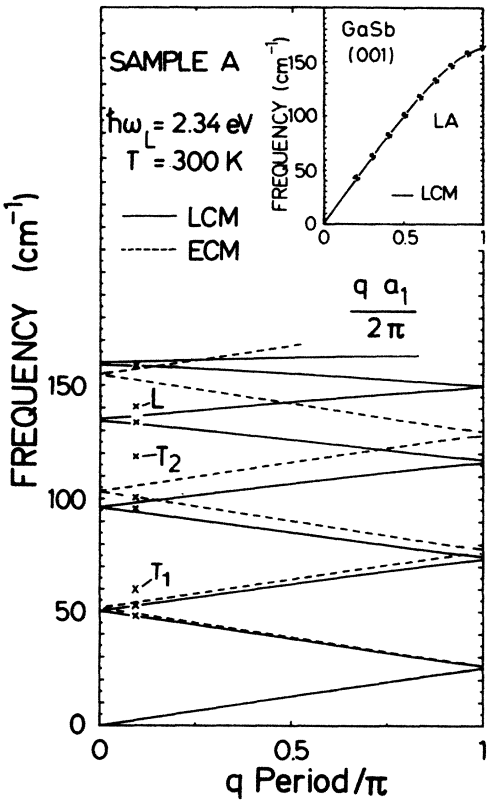

FIG. 12. Calculated folded LA dispersion based on the linear-chain model (LCM) and on the elastic-continuum model (ECM). The observed positions of the Raman lines are indicated by the crosses (×). The solid line in the inset is the LA-phonon dispersion along [001] calculated using the modified LCM described in the text. The asterisks are neutron-scattering data (from Ref. 22).

ECM explains satisfactorily the position of the first phonon doublet ($m = \pm 1$), it fails to fit the position of the higher-order folded phonons. The reason for this discrepancy lies in the nonlinearity of the LA-phonon dispersion[22,25] in the *bulk* of GaSb and AlSb for phonon wave vectors greater than $\pi/a_{1(2)}$, where $a_{1(2)}$ is the lattice constant of GaSb (AlSb) (remember that the ECM implies linear dispersion).

In order to get a more realistic dispersion, we used a modified version of the linear-chain model (LCM) with nearest-neighbor interactions described by Eq. (13) of Ref. 4. The parameters involved in this model are the anion, $M^a_{1(2)}$, and cation, $M^c_{1(2)}$, masses and the force constants between anion and cations, $K_{1(2)}$, in GaSb (AlSb). The force constants were calculated from the longitudinal sound velocities in the unstructured materials using $K_i = 8(M^a_i + M^c_i)(v_i/a_i)^2$ for each material. The values are given in Table II. In this way, the LCM reproduces well the bulk acoustic dispersion for small wave vectors ($\leq \pi/a_i$), but not the upper part of the dispersion, particularly the X-point phonon frequency.[32] This is attributed to having neglected the interactions with the second- and higher-order neighbors. To circumvent this difficulty we assumed a linear decrease of the force constants with phonon frequency from the value K_i at $\omega = 0$

to $K_i^x = M_i^a(\omega_i^x)^2/2$, where ω_i^x is the frequency of the X-point LA phonons. In this way we were able to reproduce the whole LA phonon dispersion of GaSb along [001]. This is shown in the inset of Fig. 12, where the solid line was calculated using $K_1^x/K_1 = 0.89$ and the experimental points were obtained by neutron scattering.[22] The solid line in Fig. 12 is the superlattice folded LA dispersion of sample A determined by the modified LCM described above. In the calculation, the same ratio, $K_i^x/K_i = 0.89$, was used for both GaSb and AlSb. The dispersion reproduces reasonably well the Raman shift of most of the observed Raman lines, justifying their assignment to folded-phonon doublets. Three of the lines, however, fall out of the calculated dispersion. They are labeled T_1, T_2, and L in Figs. 3, 5, and 12. The origin of these lines is not completely understood. Line T_1 (60 cm^{-1}) is observed in both configurations near resonance β (Fig. 5); its frequency corresponds to the X-point transverse-acoustic- (TA-) phonon frequency in GaSb,[22] and it may be related to the cutoff of the TA folded dispersion in the superlattice. Line T_2 has a frequency twice as large as T_1 and might be due to second-order scattering from the TA phonons. The possibility of this line coming from "mini-zone"-edge LA phonons (Ref. 33) with $q = \pi/d$ (see Fig. 12) is discarded because the corresponding zone-edge excitations have not been observed in the other branches. Finally, line L (141 cm^{-1}) is strong in both YX and XX configurations near resonance β. Its frequency agrees well with the maxima in the LA density of states in GaSb,[22] suggesting that it may also be related to scattering processes without wave-vector conservation. Such processes, involving both GaSb and AlSb phonons, might account for the large background in the Raman spectra between 130 and 165 cm^{-1}.

The Raman line at 160 cm^{-1} in Figs. 3, 5, and 6 is attributed to the folded doublet $m \pm 4$ for sample A and to $m \pm 8$ for sample B (see Fig. 4). It also corresponds to zone-edge (X-point) LA phonons in the bulk materials. This line is asymmetric with a sharp cutoff on the high-frequency side and its high intensity is probably associated with the high density of phonon states. In the bulk materials these phonons do not couple to light in first-order Raman scattering due to their large wave vector. They may, however, become Raman active in bulk through disorder-activated scattering and constitute the so-called DALA (disordered-activated LA) modes.[30]

2. *Intensity of the Raman lines*

The acoustic region of the Raman spectrum for excitation near the critical point E_1^{GaSb} (resonance α) shows intense high-order folded-LA-phonon lines in the XX configuration. For the same excitation energy a strong GaSb-like TO line appears in the YX configuration. Each pair of longitudinal-acoustic phonons with $q = 0$ belongs to the A_1 (diagonal Raman tensor) and the B_2 (off-diagonal Raman tensor) irreducible representations of the superlattice with point-group symmetry D_{2d}. The A_1 phonons produce symmetric strains and the B_2 phonons antisymmetric ones with respect to the center of the layers.[3] Hence only A_1 LA phonons will couple to light via a photoelastic (deformation-potential) mechanism, which should be dominant in off-resonance conditions.[3] Accordingly, only A_1 phonons in the XX geometry will be seen in forward scattering (wave-vector transfer $q \simeq 0$) experiments. For backscattering the q transfer is usually not zero: it has been shown[34] that at these values of q the "A_1" and "B_2" modes contain similar admixtures of the Brillouin-zone–center A_1 modes and thus have the same selection rules. Therefore, doublets are seen in XX backscattering experiments with their relative intensities depending on the value of q: the mode tending towards B_2 has vanishing intensity for $q \to 0$. This is consistent with our observation of folded-phonon doublets in the XX geometry when the excitation laser photon energy is far from resonance.

In the YX geometry, only B_2 phonons can be coupled to light. This coupling, however, cannot occur via the standard photoelastic mechanism. In order to explain our observation of folded acoustic phonons in the YX geometry (see Figs. 3–5), one has to invoke a scattering mechanism other than the long-wave photoelastic one. Colvard *et al.*[3] have suggested that the B_2 LA phonons may carry a longitudinal electric field due to the dispersion of the piezoelectric tensor and hence may couple to light. Such a mechanism may be important, particularly near resonance, as is observed in the YX spectra of Figs. 3–5.

The intensities of the folded acoustic phonons have been calculated for photoelastic coupling in the elastic continuum limit.[14] These predictions were checked for GaAs/AlAs superlattices, where the photoelastic coefficients were assumed to be constant within each layer.[14] In a first approximation, where the differences in the acoustic impedances of the layers is neglected, the intensity of the mth acoustic-phonon doublet is proportional to the square of the mth Fourier component of the photoelastic coefficient.[4] This coefficient describes the phonon-induced modulation of the electronic susceptibility and is periodically modulated along the superlattice growth direction following the alternation of layers. The change in the relative amplitude of the folded-phonon doublets with the laser excitation energy indicates that the photoelastic coefficients cannot depend only on the artificial periodicity as assumed in the photoelastic model.[14] Rather, they must be further modulated by the spatial variation of the electronic wave function $\varphi(z)$ of the intermediate state for the Raman process. In particular, the increase in amplitude of the higher-order folded-phonon lines for laser photon energies near resonance α implies a corresponding increase in the higher-order Fourier components of $\varphi(z)$.

For laser excitation energies below $E_0^{AlSb,SL}$ the real electronic transitions in Raman scattering, and therefore the wave function $\varphi(z)$, are confined to the GaSb layers and decay exponentially in the AlSb layers. As $E_0^{AlSb,SL}$ is approached, it is expected that $\varphi(z)$ penetrates the AlSb layers. An oscillatory behavior of $\varphi(z)$ within the GaSb layers with period $m(\pi/d_1)$ ($m = 1,2,\ldots$), similar to that found in quantum wells, could, in principle, account for the high intensity of the higher-order acoustic folded doublets. This, however, should be followed by a

corresponding enhancement of the higher-order GaSb-like confined optical-phonon lines that has not been observed. Alternatively, $\varphi(z)$ can concentrate at the layer interfaces for $\hbar\omega_L$ between E_1^{GaSb} and $E_0^{\mathrm{AlSb,SL}}$. Above $E_0^{\mathrm{AlSb,SL}}$ this confinement effect should disappear as the wave function extends over the AlSb layers. The confinement of the wave function near the interfaces would then account for the high-order Fourier component of the electronic density and therefore for the appearance of the high-order folded-phonon doublets in the Raman spectrum.[35]

Finally, as the interfaces are the joining planes of two different lattices, they are expected to have some roughness and the material to be of less crystalline quality than within the layers. The interface roughness provides a way of coupling light to modes that propagate along the superlattice interfaces and that are forbidden in backscattering Raman experiments. This is the case for the interface modes discussed in Sec. III B 3. Such a mechanism could also account for the observation of the strong GaSb-like TO line for excitation near E_1^{GaSb}, which should be forbidden in backscattering geometry. Furthermore, the disorder in the interface region may relax the momentum-conservation rule for Raman scattering and render Raman-active modes that cannot couple to light in a perfect crystal. The confinement of the electronic wave function at the interfaces would enhance the intensity of these disorder-activated modes. This mechanism could, in principle, account for the high intensity of the lines $m\pm4$ ($m\pm8$ in sample B), T_1, T_2, and L, and also for the large background between 130 and 165 cm^{-1} in the Raman spectra with laser excitation near $E_1^{\mathrm{GaSb,SL}}$. All these lines are related to maxima in the phonon density of states and are associated with scattering processes without wave-vector conservation.

IV. SUMMARY

We have observed a number of unusual features in the folded acoustic phonons in short-period GaSb/AlSb superlattices. A quantitative understanding of these features is still lacking. Confined optical phonons and interface modes were also studied. It would be worthwhile to carry out a detailed resonance Raman study of acoustic phonons in short-period GaSb/AlSb superlattices.

Finally, it has come to our attention that the vibrations of GaSb/AlSb superlattices have also been recently investigated by G. P. Schwartz and collaborators.[36]

ACKNOWLEDGMENTS

We would like to thank M. Garriga for performing the ellipsometric measurements and interpreting the results, L. Tapfer and W. Stolz for x-ray determination of sample parameters, and W. Kauschke for helpful comments and suggestions. We also acknowledge the technical assistance of M. Siemens, H. Hirt, and P. Wurster.

*Present address: Materials Science Laboratory, Indira Ghandhi Centre of Atomic Research, Kalpakkam 603 102, Tamilnadu, India.

[1]For a recent review, see M. V. Klein, IEEE J. Quantum Electron. **QE-22**, 1760 (1986).

[2]M. Cardona, in *Lectures on Surface Science*, edited by G. R. Castro and M. Cardona (Springer-Verlag, Heidelberg, 1987), p. 2.

[3]C. Colvard, R. Merlin, M. V. Klein, and A. C. Gossard, Phys. Rev. Lett. **45**, 298 (1980).

[4]C. Colvard, T. A. Grant, M. V. Klein, R. Merlin, R. Fisher, H. Morkoç, and A. C. Gossard, Phys. Rev. B **31**, 2080 (1985).

[5]B. Jusserand, D. Paquet, and A. Regreny, Phys. Rev. B **30**, 6245 (1984).

[6]A. K. Sood, J. Menéndez, M. Cardona, and K. Ploog, Phys. Rev. Lett. **54**, 2111 (1985).

[7]A. K. Sood, J. Menéndez, M. Cardona, and K. Ploog, Phys. Rev. Lett. **54**, 2115 (1985).

[8]B. Jusserand, P. Voisin, M. Voos, L. L. Chang, E. E. Mendez, and L. Esaki, Appl. Phys. Lett. **46**, 678 (1985).

[9]J. M. Calleja, F. Meseguer, C. Tejedor, E. E. Mendez, C. A. Chang, and L. Esaki, Surf. Sci. **168**, 558 (1986).

[10]E. E. Mendez, C. A. Chang, H. Takaoka, L. L. Chang, and L. Esaki, J. Vac. Sci. Technol. B **1**, 152 (1983).

[11]G. Griffiths, K. Mohammed, S. Subbana, H. Kroemer, and J. Merz, Appl. Phys. Lett. **43**, 1059 (1983); K. Ploog, Y. Ohmori, H. Okamoto, W. Stolz, and J. Wagner, *ibid.* **47**, 384 (1985).

[12]P. Voisin, G. Bastard, M. Voos, E. E. Mendez, C. A. Chang, L. L. Chang, and L. Esaki, J. Vac. Sci. Technol. B **1**, 409 (1983).

[13]F. Tejedor, J. M. Calleja, F. Meseguer, E. E. Mendez, C. A. Chang, and L. Esaki, Phys. Rev. B **32**, 5303 (1985).

[14]B. Jusserand, D. Paquet, F. Mollot, F. Alexandre, and G. Le Roux, Phys. Rev. B **35**, 2808 (1987).

[15]S. M. Rytov, Akust. Zh. **2**, 71 (1956) [Sov. Phys.—Acoust. **2**, 68 (1956)].

[16]L. Tapfer and H. Stolz (private communication).

[17]T. P. Pearsall, F. H. Pollak, J. C. Bean, and R. Hull, Phys. Rev. B **33**, 6821 (1986).

[18]*Landolt-Börnstein Tables*, edited by K.-H. Harbeke, O. Madelung, and U. Rössler (Springer, Berlin, 1982), New Series, Group III, Vol. 17a.

[19]T. Nakayama and H. Kamimura, J. Phys. Soc. Jpn. **54**, 4726 (1985).

[20]M. Garriga, M. Cardona, N. E. Christensen, P. Lautenschlager, T. Isu, and K. Ploog, Phys. Rev. B **36**, 3254 (1987).

[21]J. M. Calleja, H. Vogt, and M. Cardona, Philos. Mag. A **45**, 239 (1982).

[22]M. K. Farr, J. G. Traylor, and S. K. Sinha, Phys. Rev. B **11**, 1587 (1975).

[23]W. Kauschke, N. Mestres, and M. Cardona, Phys. Rev. B **36**, 7469 (1987).

[24]P. Voisin, C. Delalande, M. Voos, L. L. Chang, A. Segmuller, C. A. Chang, and L. Esaki, Phys. Rev. B **30**, 2276 (1984); F. H. Pollak and M. Cardona, Phys. Rev. **172**, 816 (1968).

[25]See compiled data in H. Bilz and W. Kress, *Phonon Dispersion Relation in Insulators* (Springer, Heidelberg, 1979).

[26]R. Banerjee and Y. P. Varshni, Can. J. Phys. **47**, 451 (1968).
[27]F. Cerdeira, C. J. Buchenauer, F. Pollak, and M. Cardona, Phys. Rev. B **5**, 580 (1972).
[28]E. Anastassakis and M. Cardona, Solid State Commun. **63**, 893 (1987).
[29]B. Jusserand and D. Paquet, Phys. Rev. Lett. **56**, 1752 (1986); A. K. Sood, J. Menéndez, M. Cardona, and K. Ploog, *ibid.* **56**, 1753 (1986).
[30]E. Bedel, R. Carles, A. Zwick, J. B. Renucci, and M. A. Renucci, Phys. Rev. B **30**, 5923 (1984).
[31]D. E. Aspnes and A. A. Studna, Phys. Rev. B **27**, 985 (1983).
[32]D. N. Talwar and B. K. Agrawal, Phys. Rev. B **8**, 693 (1973).
[33]J. Sapriel, J. Chavignon, F. Alexandre, and R. Azoulay, Phys. Rev. B **34**, 7118 (1986).
[34]J. Sapriel, J. C. Michel, J. C. Toledano, R. Vacher, J. Kervarec, and A. Regreny, Phys. Rev. B **28**, 2007 (1983).
[35]T. Suemoto, G. Fasol, and K. Ploog, Phys. Rev. B **34**, 6034 (1986).
[36]G. P. Schwartz, G. J. Gualtieri, W. A. Sunder, and L. A. Farrow, Phys. Rev. B **36**, 4868 (1987).

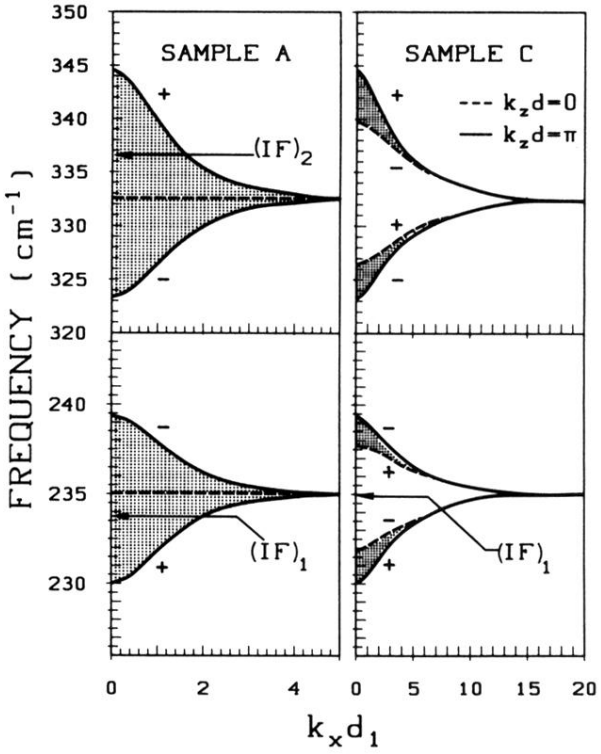

FIG. 11. Calculated dispersion of interface vibrational modes based on electrostatic model (Ref. 7). The observed modes $(IF)_1$ and $(IF)_2$ are indicated by arrows.